Defence Science Journal, Vol. 73, No. 3, May 2023, pp. 283-292, DOI : 10.14429/dsj.73.17735

Aerodynamic Investigation of Blended Wing Body Configuration

Midhun M.V., Partha Mondal*, Pawan Kumar Karn and Priyank Kumar

Department of Space Engineering and Rocketry, Birla Institute of Technology, Mesra, Ranchi - 835 215, India
**E-mail: pmondal@gmail.com*

ABSTRACT

A blended wing body (BWB) configuration is an unconventional aircraft design in which the wing and fuselage are blended to form an aircraft. This design concept has inherent higher aerodynamic efficiency, environmental benefits and capacities. These advantages make the BWB configuration a feasible concept for commercial transport aircraft. In the present work, a 3-D BWB model is designed in SolidWorks and fabricated using a 3D printer. The numerical and experimental analyses are carried out with this BWB geometry. Aerodynamic characteristics and flow features obtained from the open-source CFD software OpenFOAM have been studied, analyzed, and compared with the wind tunnel results. Experimental and computational data compare well and the present BWB can operate at a high angle of attack. The coefficient of lift (C_L) increases with AoA up to 45º. The C_L starts decreasing beyond this AoA, and the present BWB geometry stalls at around AoA = 45º. The coefficient of drag (C_D) increases with the increase in AoA due to the spreading of the separated region over the geometry. Lift/Drag (L/D) variation with AoA is also studied to find the optimum flight configuration of the present BWB geometry. Sectional pressure distribution at different spanwise locations, velocity contours, pathlines, surface limiting streamlines and tuft flow visualization are also presented to investigate the flow. The studies investigate the aerodynamics, flow field and optimal flight configuration for cruising a BWB geometry.

Keywords: Blended wing body; Aerodynamics; OpenFOAM; Flow visualisation; Wind tunnel

1. INTRODUCTION

Blended wing body configuration merges the fuselage with the wing and eliminates the tail. Since the wing is blended smoothly to form a wide flat fuselage, this fuselage produces most of the lift. Studies have shown that BWB configuration can reduce fuel burn significantly, hence reducing operating costs. Also, it has shown promising aerodynamic efficiency with the entire aircraft generating the lift with minimum drag, thus increasing the fuel economy and range[1-2].

With the elimination of the tail and transformation of it into a single lifting body, the wetted area-to-volume ratio is also reduced which leads to interference drag reduction. The BWB configuration also offers environmental and some unique safety advantages. By placing the engines above the wing, the engine noise will not interact with the wing's lower surface, hence having a low acoustic signature.

Despite the numerous advantages of the BWB configuration, certain challenges exist. For instance, one of the crucial aspects of the BWB is stability and control. This is owing to the elimination of the tail as well as the unconventional shape of the aircraft. Designing and allocation of the control surfaces are crucial. Also, since the BWB is a blend of fuselage and wing, specifying a center body structure becomes a challenge. As a result, it is required to carefully design and optimize the fuselage section to accomplish the aerodynamic and structural requirements.

In the late 90s, Potsdam[2], *et al.* presented the BWB unconventional configuration which offered great advantages in terms of performance over conventional, transonic transports. Roberto Merino-Martinez[3] designed a BWB baseline configuration and studied the aerodynamic performance. Also, he performed the Euler-based shape optimization considering its challenging stability and control features**.** Qin[5], *et al.* discussed the BWB configuration, which is designed under the European project, MOB. Richard J. Re[6] investigated a BWB subsonic transport configuration to get the aerodynamic coefficients and pressure distribution over the wing. Ammar[7], *et al.* designed a 200 passengers capacity BWB aircraft and compared its aerodynamic performance with A320 aircraft with an emphasis on the stability of the plane.

Dehpanah[10], *et al.* investigated the aerodynamic aspects of different blended wing body airframes using computational analysis. Thompson[11], *et al.* designed and constructed a 5m wingspan autonomous BWB UAV. Roman[12], *et al.* developed a BWB configuration to determine its feasibility at transonic speeds, from M=0.85 to M=0.93. The model was first analyzed using CFD, optimized in WingMOD. Lyu[13], *et al.* performed aerodynamic shape optimization for a BWB aircraft using RANS with the Spalart-Allmaras turbulence model.

Okonkwo[14], *et al.* reviewed the evolving trends in the design and challenges faced during the design of the BWB aircraft. Kuntawala[15], *et al.* presented the flow analysis and aerodynamic shape optimization of BWB configuration**.** Larkin[16], *et al.* analyzed the stability of a BWB configuration

---

Received : 01 December 2021, Revised : 03 December 2022
Accepted : 03 February 2023, Online published : 12 May 2023

with vertical stabilizers. Zhang[17]*, et al.* presented an optimization technique to minimize the cruise drag at transonic speed for a BWB transport. Siouris[18]*, et al.* numerically investigated the aerodynamic performance of a BWB with different wing sweeps. Howe[19] developed a method to predict the airframe mass of blended wing body designs. Nguyen[20]*, et al.* presented the multidisciplinary design optimization procedure to design unmanned combat air vehicles using a multi-fidelity model. The efficient stall prediction method is predicted and validated with wind tunnel data by Nguyen[21]*, et al.* Torenbeek[22] discussed the historical development of BWB and its challenges and advantages.

Vicroy*, et al.*[23] studied the aerodynamic characteristics of BWB at low speed with a tri-jet configuration. Wisnoe[24]*, et al.* studied the aerodynamic behavior of unmanned aerial vehicles using CFD and wind tunnel experiments for low subsonic speeds. Nasir[25]*, et al.* investigated the aerodynamics, stability, and flying quality of a BWB with a canard configuration. Brown[26]*, et al.* presented the conceptual design of BWB aircraft and compared it with tube-and-wing aircraft. Zadeh[27]*, et al.* developed an optimization model for BWB UAVs.

Lyu[28]*, et al.* studied the influence of the winglet on the hydrodynamic performance of BWB. Zhang[29]*, et al.* investigated the effects of stability margin and thrust specific fuel consumption on the design of BWB. Viviani[30]*, et al.* presented the low-speed longitudinal performance of a BWB re-entry vehicle. The scale effects of BWB civil aircraft were investigated by Wang[31]*, et al.* Kapsalis[32]*, et al.* studied tactical BWB UAV layout optimization using CFD and Taguchi experimental methods.

Most of the papers available in the literature on BWB configuration discussed aerodynamic shape optimization. In the present work, an aerodynamic investigation of a BWB configuration is performed at low subsonic speed. This study set out to investigate the aerodynamic coefficients, flow field over the geometry, and optimal flight configuration in cruise. A 3-D BWB model is designed in SolidWorks and fabricated using a 3D printer. The computational analysis is carried out using the open-source software OpenFOAM[8], and the wind tunnel experiments are performed at an air speed of 20m/s. In both analyses, aerodynamic coefficients are evaluated with respect to the change in angle of attack (AoA). Pressure distribution, pathlines, and limiting streamlines on the surface of the BWB model are also extracted from the CFD data to study the flow over the 3D model. Tuft flow visualization is performed to observe the flow pattern over the BWB at various angles of attack.

2. METHODOLOGY

Step 1: Designing and Fabrication of the BWB Model

The current BWB model design is inspired by some of the measurements in the thesis of Roberto Merino Martinez[3], and the aerofoil selections are based on the paper of Carlsson[4]*, et al.* This geometry is made of the center body and inner and outer wings, which are then merged to form the BWB. The propulsion systems are not included in the current BWB design. The BWB model consists of two aerofoil profiles, NACA 0017 and NACA 0012, which are placed in 6 different sections, defining the geometry.

- NACA 0017, the center of the model, from 0 mm to 0.35 mm.
- NACA 0017, from 0.35 mm to 41.5 mm, comprising the fuselage
- NACA 0012, from 41.5 mm to 52.28 mm, inner wing
- NACA 0012, from 52.28 mm to 62.35 mm, inner wing
- NACA 0012, from 62.35 mm to 82.21 mm, comprising the outer wing
- NACA 0012, at the tip of the wing

The airfoil coordinates were generated using the airfoil generator of Airfoil Tools[9]. Figure 1 shows the BWB model for the present analysis. Table 1 shows the specifications of the current BWB model. The reference area for calculating the aerodynamic coefficients is mentioned in Table 1.

The model used for experiments is fabricated using a 3D Printer. The designed CAD model is imported into the software for 3D printing. The fused filament fabrication (FFF) process is used for the fabrication, and the material used is Acrylonitrile Butadiene Styrene (ABS) plastic. The BWB model is printed in two halves and then combined to form the whole geometry. The model is then coated with some layers of spray paint to increase the smoothness of the surface. The half model is used for the computational analysis, whereas the experiments are carried out using the full model.

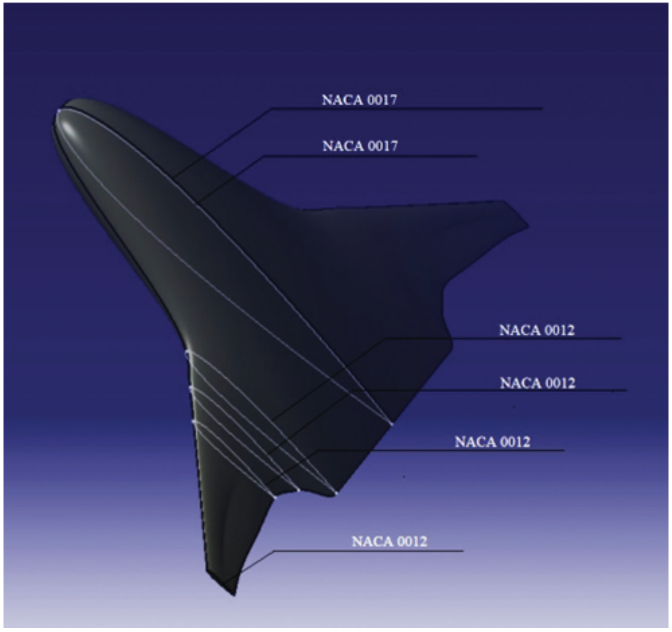

Figure 1. Blended wing body (BWB) model.

Table 1. Specifications of the present BWB model

Root chord length	157.14 mm
Span	215.85 mm
Aspect ratio	3.2
Reference area	14547 mm^2
Sweep angle (1st)	71.66^o
Sweep angle (2nd)	38.52^o

Step 2: CFD Analysis

A C-type structured grid is generated over the BWB geometry using the commercial software GAMBIT. Half of the model is taken for the computational analysis. The far field is located at 20 times the root chord of the blended wing body. Grid stretching is used to concentrate the mesh accordingly over the model and domain. The grid is hexahedral in the domain except at the wing tip region where hex/wedge type with cooper scheme is used. The boundary conditions specified for the grid are shown in Fig. 2(a). The dimensionless wall distance y+ of the first point located off the wall is 50. The mesh contained 2.1 million cells and was generated considering the use of a wall function[36]. The zoomed view of the mesh over the model can be seen in Fig. 2(b). The details of the boundary conditions used for CFD simulation are tabulated in Table 2.

The numerical simulation is performed using an open-source CFD software OpenFOAM[8]. The simulation is carried out for a steady-state, incompressible flow with a velocity of 20 m/s corresponding to the Reynolds Number of 2.1×10^5 based on the root chord. The simpleFoam solver is used with Spalart-Allmaras[33] turbulence model for the present simulation. Aerodynamic characteristics such as C_L and C_D at various angles of attack are computed, and velocity contours and pathlines are obtained from the simulated data.

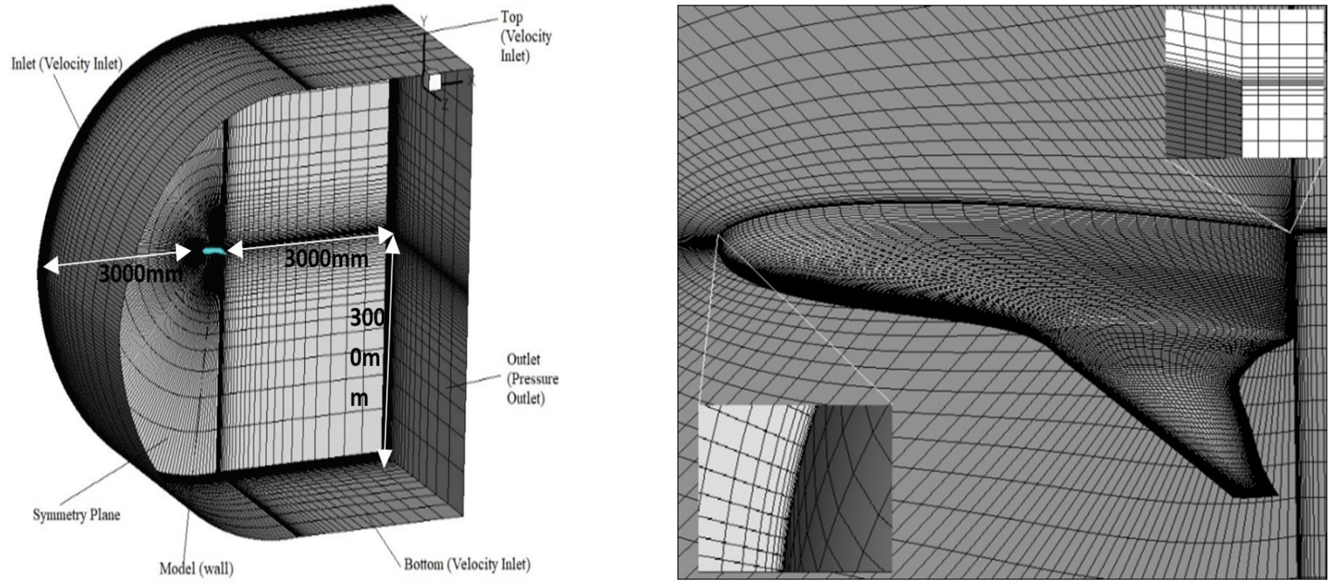

(a) Boundary conditions

(b) Closer view of the mesh

Figure 2. Boundary conditions and grid of the present simulation.

Table 2. Boundary conditions used in CFD simulation

	Boundary conditions
Inlet	Velocity inlet
Top	Velocity inlet
Bottom	Velocity inlet
Outlet	Pressure outlet
Symmetry plane	Symmetry
BWB model	Wall (No slip)

Step 3: Experimental Analysis

All experiments are conducted using the low subsonic wind tunnel available at the Aerodynamic Lab., Department of Space Engineering and Rocketry, BIT Mesra, Ranchi. The test section of this tunnel is 600 mm x 600 mm x 1200 mm. It is a suction-type, open circuit continuous flow fan-driven wind tunnel. Quantitative and qualitative analyses are performed at different AoA to study the flow physics of the BWB model. Quantitative analysis includes the measurement of forces using strain gauge balance. Qualitative research is done using the tuft flow visualization technique. Experiments are carried out on the 3-D blended wing body model fabricated using a 3-D printer.

Figure 3. BWB model placed in the wind tunnel.

Figure 3 shows the BWB model placed in the wind tunnel for the force measurements. The experiments are performed at a velocity of 20m/s and Reynolds number of 2.1×10^5 based on the root chord from $\alpha=0^o$ to $\alpha=50^o$ with an increment of 5º step. The wind tunnel blockage was found to be less than 5% at maximum AoA. A 5-component internal strain gauge balance was used. An external power supply of 3 V was used for the excitation of bridges. The data were acquired at a sampling frequency of 100 Hz. The acquired data was filtered using a low pass filter of 10 Hz[34].

3. RESULTS AND DISCUSSIONS

This section presents the results obtained from the CFD and experimental analyses of the blended wing body configuration. The results obtained are analyzed and discussed to understand the flow behavior over the BWB model. The computational results are also compared with experimental data.

The performance of two different turbulence models is analyzed, and the comparison of the computational data with the experiment at an angle of attack 20^0 is shown in Table 3. At high AoA, the flow separates over the BWB surface. Therefore, the predicted aerodynamic coefficients by the turbulence models will not be very accurate as AoA increases. In the present work, the Spalart-Allmaras turbulence model is chosen for the flow simulation as this is one of the suitable turbulence models for external aerodynamics[35].

Table 3. Comparison of aerodynamic coefficients using different turbulence models with experiment at AoA = 20^0

	C_L	C_D
Spalart-Allmaras turbulence model	0.742	0.232
k-ω SST turbulence model	0.794	0.245
Experiment	0.710	0.289

3.1 Aerodynamic Characteristics of BWB

3.1.1 Force Coefficients

Aerodynamic force coefficients, which include the lift and the drag coefficients acting over the model, are presented for the different angles of attack (α).

Figure 4(a) depicts the lift coefficient (C_L) variation for different AoA varying from 0º to 60º. The lift coefficient increases with the increase in AoA up to 45º. Increasing the AoA beyond 45º, the flow will fully separate from the body. At this point, the C_L starts decreasing with increasing AoA, and the body is said to be stalled. This suggests that the present BWB model is stalled at around α = 45º. Among the geometric parameters, a high sweepback angle is responsible for this type of stall behavior.

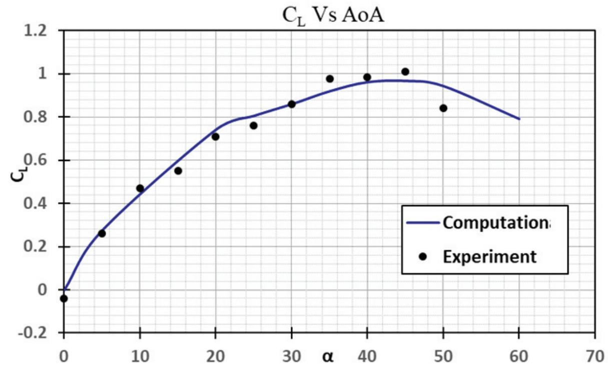

(a) Variation of C_L with angle of attack

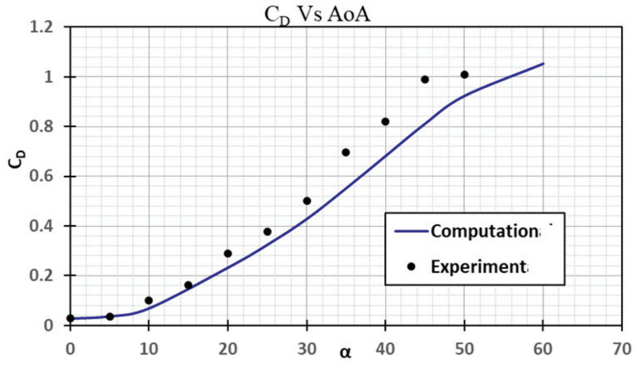

(b) Variation of C_D with the angle of attack

Figure 4. C_L and C_D variations with the angle of attack.

Figure 4(b) shows the variation of the drag coefficient (C_D) for different AoA varying from 0º to 60º. At low AoA (α < 5º), the value of C_D is small, and its variation is not significant with increasing the AoA. As the AoA is increased beyond α = 5º, the C_D continues to increase due to the spreading of the separated region over the upper surface of the BWB model.

The computational results match well with the experimental data. However, at higher AoA, computational values start deviating from the experimental data, particularly in drag prediction.

3.1.2 Lift/Drag Ratio and Drag Polar

Figure 5(a) shows the variation of the lift-to-drag ratio (L/D) for different AoA (α) obtained from the computational and experimental analyses. The maximum value of L/D is around 8, and it is achieved at an AoA 6º. Hence, the optimum flight configuration of the present BWB body will be at α = 6º for better aerodynamic performance. This maximum L/D ratio is relatively smaller than the desired value for low-speed aircraft, which is occurred due to the small lift curve slope with a high drag coefficient.

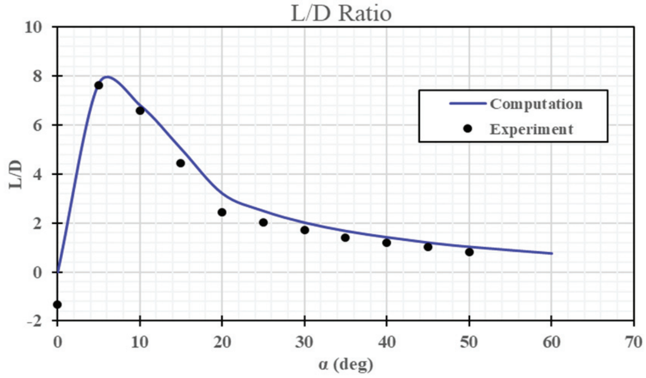

(a) Variation of L/D with angle of attack

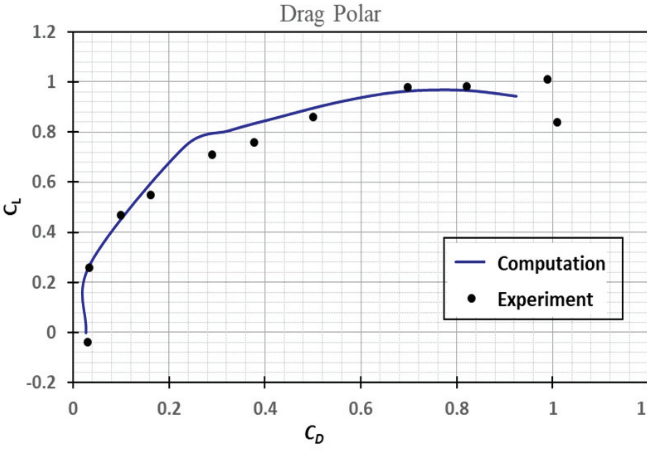

(b) Drag Polar for the BWB

Figure 5. L/D variation and drag polar for the BWB.

Figure 5(b) shows the drag polar for the BWB model. Initially, the CL change is sharp, and then it increases gradually. On the other hand, C_D increases sharply at a large angle of attack, which prevents the L/D to reach its maximum value. The maximum L/D can be attained by drawing a tangent to the curve starting from the origin. The low aspect ratio of the model increases the induced drag. Also, at a large angle of attack, the separated region is increased, which increases the pressure drag. Therefore, the total drag acting on the model is increased with AoA.

3.2 Pressure Coefficient Distribution

The coefficient of pressure (-Cp) distributions are plotted at four different specified spanwise locations (z/(b/2)): 0.1, 0.5, 0.7, and 0.9 for the BWB model for various angles of attack. Pressure coefficient distributions at spanwise locations for different angles of attack are shown in Fig. 6 and 7.

3.2.1 Section at z/(b/2) = 0.1

The pressure coefficient (-Cp) is computed at 10 % of the semi-span location. The aerofoil in this section is NACA 0017. At 0º angle of attack, since the aerofoil used is symmetric, Cp distributions on the upper and lower surfaces coincide with each other. This can be observed at all spanwise locations, as shown in Fig. 6. At this section (z/(b/2) = 0.1) and α = 0º, the pressure coefficient increases sharply till around 16% of the chord location and then decreases till the trailing edge, as shown in Figure 6(a).

At α = 40º (Fig. 7(a)), the pressure coefficient sharply increases near the leading edge on the upper surface, decreases gradually till 40 % of the chord, then increases to approximately 50 % of the chord, and finally decreases to become same pressure coefficient of the lower surface at the trailing edge. On the other hand, the pressure coefficient starts decreasing approximately 40% of the chord on the lower surface and then increases gradually till the trailing edge of the airfoil.

3.2.2 Section at z/(b/2) = 0.5

The pressure coefficient (-Cp) at α = 0º and 50 % of the semi-span location is shown in Fig. 6(b). The aerofoil in this section is NACA 0017. Due to the symmetric airfoil, the pressure distributions on upper and lower surfaces coincide at α = 0º. In this section, the pressure coefficient increases approximately till 25% of the chord and then decreases till the trailing edge of the airfoil. At α = 40º (Fig. 7(b)), the pressure coefficient increases sharply at the leading edge and decreases approximately till 5 % of the chord on the upper surface and then remains almost constant till the trailing edge of the airfoil. This constant pressure distribution is due to the large separated region on the upper surface of the wing. The lower surface pressure coefficient distribution starts decreasing at approximately till 10 % of the chord and then increases gradually till the trailing edge of the airfoil.

3.2.3 Section at z/(b/2) = 0.7

The aerofoil in this section is NACA 0012. At α = 0º and 70% of the semi-span location, the pressure coefficient (-Cp)

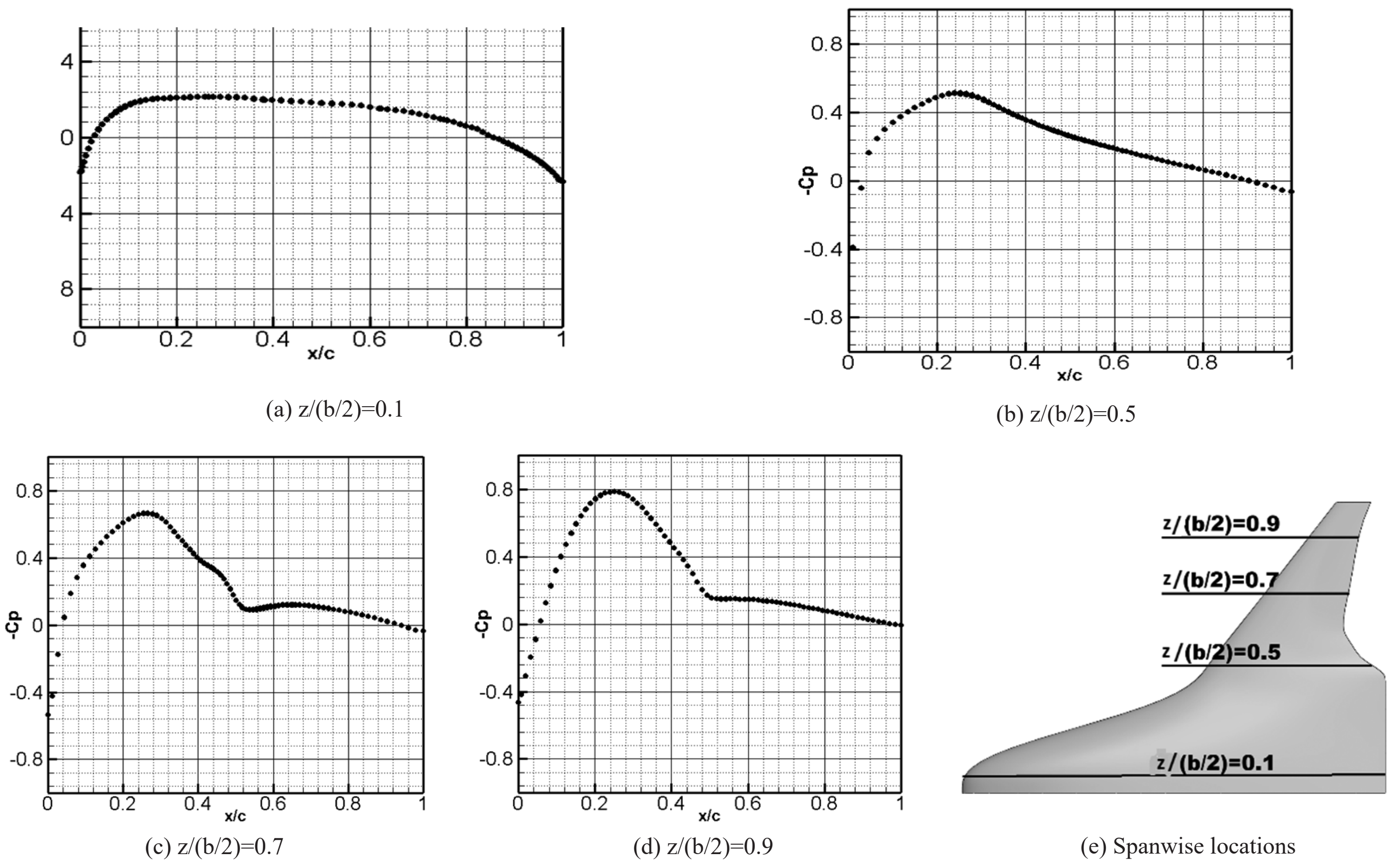

(a) z/(b/2)=0.1

(b) z/(b/2)=0.5

(c) z/(b/2)=0.7

(d) z/(b/2)=0.9

(e) Spanwise locations

Figure 6. Pressure coefficient (-Cp) distribution at indicated spanwise locations (AoA = 0^0).

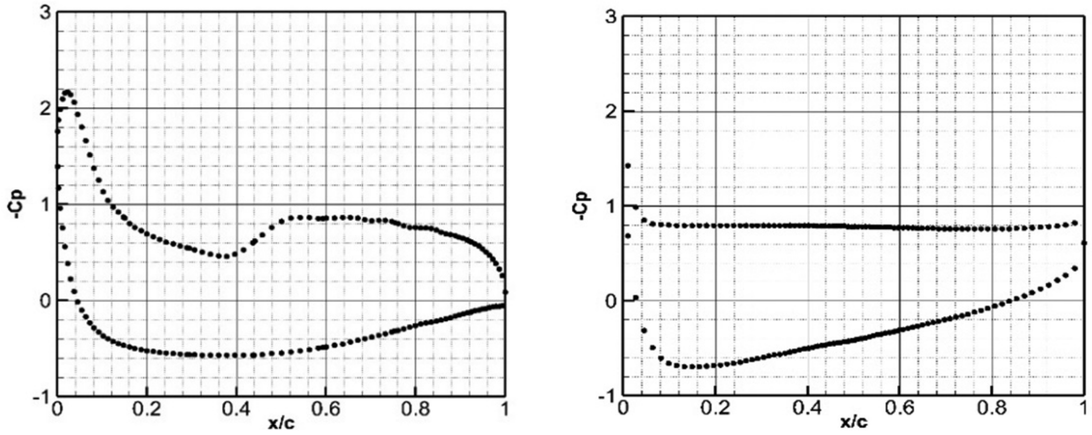

(a) z/(b/2)=0.1 (b) z/(b/2)=0.5

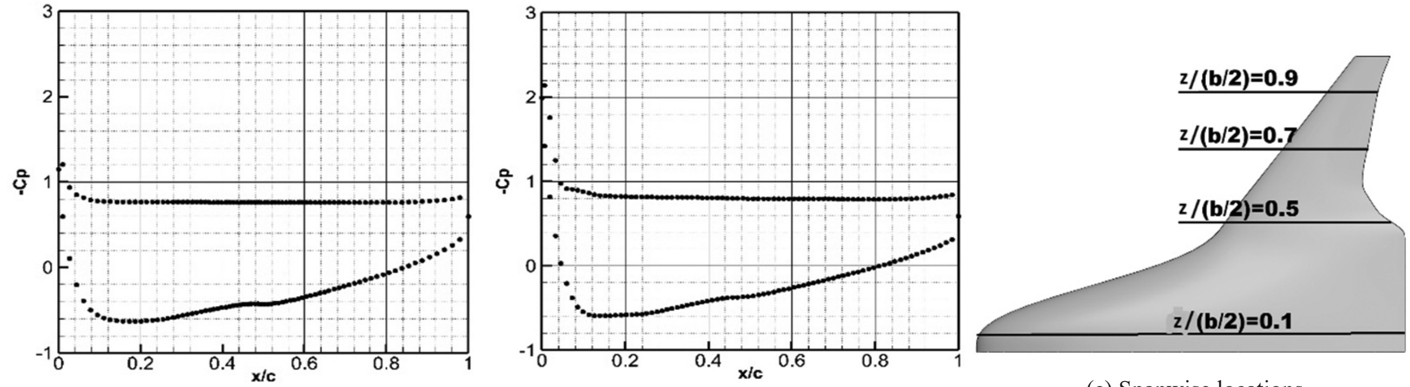

(c) z/(b/2)=0.7 (d) z/(b/2)=0.9 (e) Spanwise locations

Figure 7. Pressure coefficient (-Cp) distribution at indicated spanwise locations (AoA = 40°).

is shown in Fig. 6(c). The pressure coefficient distributions on upper and lower surfaces coincide due to the symmetric airfoil. The pressure coefficient increases at approximately till 30 % of the chord, then decreases at approximately till 50 % of the chord, and finally, it gradually decreases till the trailing edge of the airfoil. At α = 40º (Fig. 7(c)), the trend is similar as it was observed at z/(b/2) = 0.5 for the same angle of attack. The pressure coefficient increases sharply at the leading edge and decreases approximately till 8% of the chord on the upper surface and then remains constant till the trailing edge of the airfoil. This constant pressure distribution is due to the fully separated region at the upper surface of the wing, and the wing is stalled. The lower surface pressure distribution also looks similar to the pressure distribution as observed for z/(b/2) at 0.5 and α = 40º.

3.2.4 Section at z/(b/2) = 0.9

This section is near the wing tip, and the airfoil profile is NACA 0012. The trends of the pressure coefficient (-Cp) distributions in this section (Figures 6(d) and 7(d)) are similar as it was observed at z/(b/2) = 0.7 for the respective angle of attack. But the peaks of pressure coefficients and their locations are different as compared to the values at z/(b/2) = 0.7.

3.3 Flow Visualizations

3.3.1 Pathlines at Different Angles of Attack

The flow over the BWB model changes with the increase in the AoA. To visualize the flow behavior over the BWB model, velocity contours and pathlines of the flow are created. Fig. 8 shows the velocity contour and pathlines over the model at different AoA.

At α = 0º, the flow over the model leaves smoothly, as shown in Fig. 8(a) and 8(c). The flow is attached to the surface of the model, and no lift is produced as the aerofoils are symmetrical.

At α = 40º, the flow will separate all over the body. The vortex starts lifting off the body in the circulation zone. The flow will be vortical over the surface of the body. The vortical structure of the flow at higher AoA α = 40^0 is shown in Fig. 8(b) and 8(d).

3.3.2 Streamlines over the BWB at Different Angles of Attack

Streamlines are visualized on the upper surface of the BWB model to get a better understanding of the flow over the model at different AoA. Figure 9 shows the surface limiting streamlines over the BWB model at different AoA.

At AoA 0º, the streamlines are straight and attached to the body, as shown in Fig. 9(a). The flow will start to separate with an increase in the AoA. At AoA 40º, the separated region is increased. Increasing the AoA, the vortices are spreading up over the body. This can be observed from the streamlines, as shown in Fig. 9(b).

3.3.3 Tuft Flow Visualisation

Visualisation using tuft during wind tunnel tests is

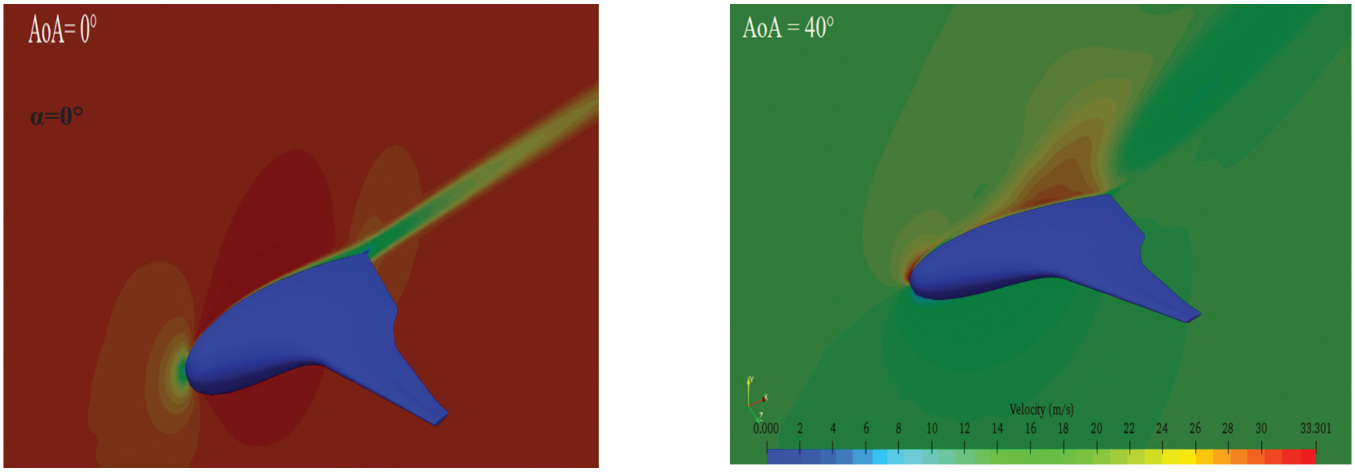

(a) Velocity contours, AoA = 0^0

(b) Velocity contours, AoA = 40^0

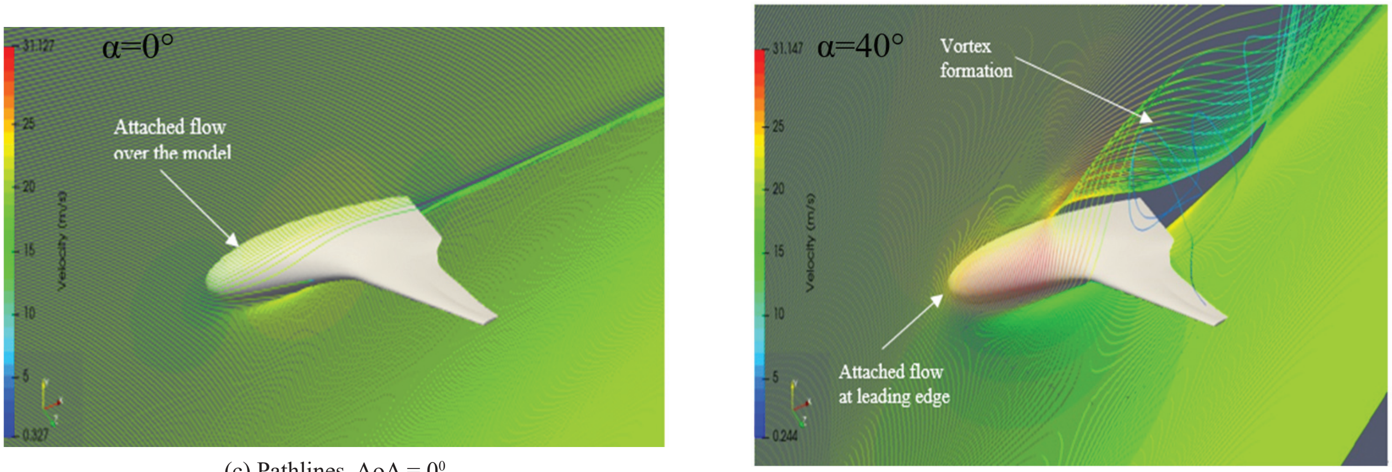

(c) Pathlines, AoA = 0^0

(d) Pathlines, AoA = 40^0

Figure 8. Velocity contours and pathlines over the BWB model at different angles of attack.

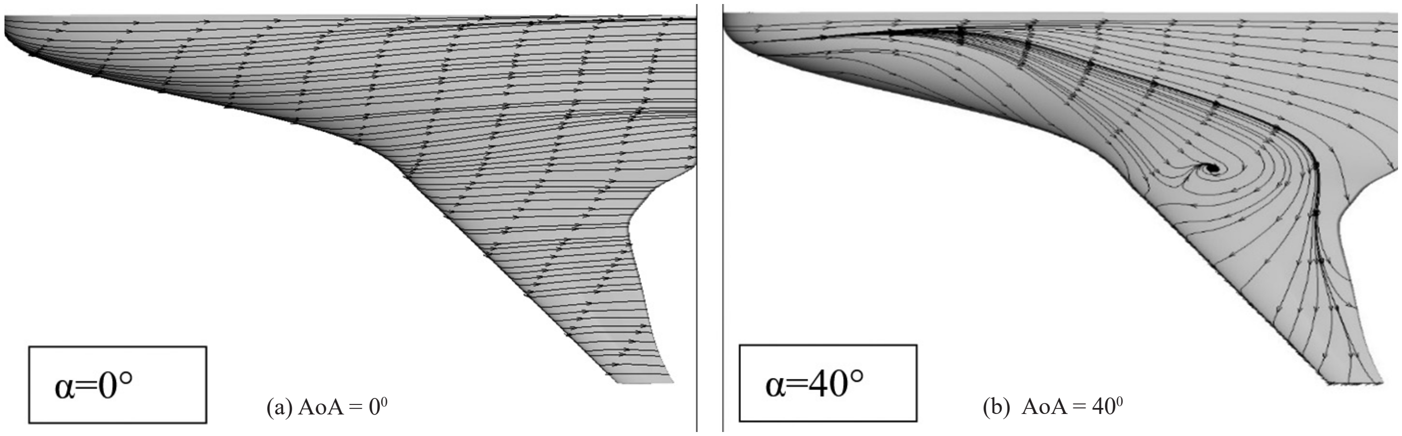

(a) AoA = 0^0

(b) AoA = 40^0

Figure 9. Surface streamlines over the BWB model at different angles of attack.

also performed in the present analysis. Tufts will align itself accordingly as air flows over the model. The tuft flow visualization was carried out for the angle of attack from 0º to 50º. Figure 10 shows the tuft flow at AoA 0º and 50º.

At AoA 0º, the tufts are arranged in the direction of the flow all over the model, as shown in Fig. 10(a). At α = 50º, the tufts all over the model oscillate. Hence the flow is fully vortical over the model (Fig. 10(b)).

4. CONCLUSIONS

Blended-wing-body (BWB) configuration is an innovative idea in which the wing and body are blended to form an aircraft. This BWB configuration has several benefits from its inherent aerodynamic potential. In this work, the aerodynamic performance of a BWB geometry is studied both numerically and experimentally at a low subsonic speed. Both the numerical and experimental data compare well. For this purpose, a 3-D BWB geometry is designed using SolidWorks. This designed

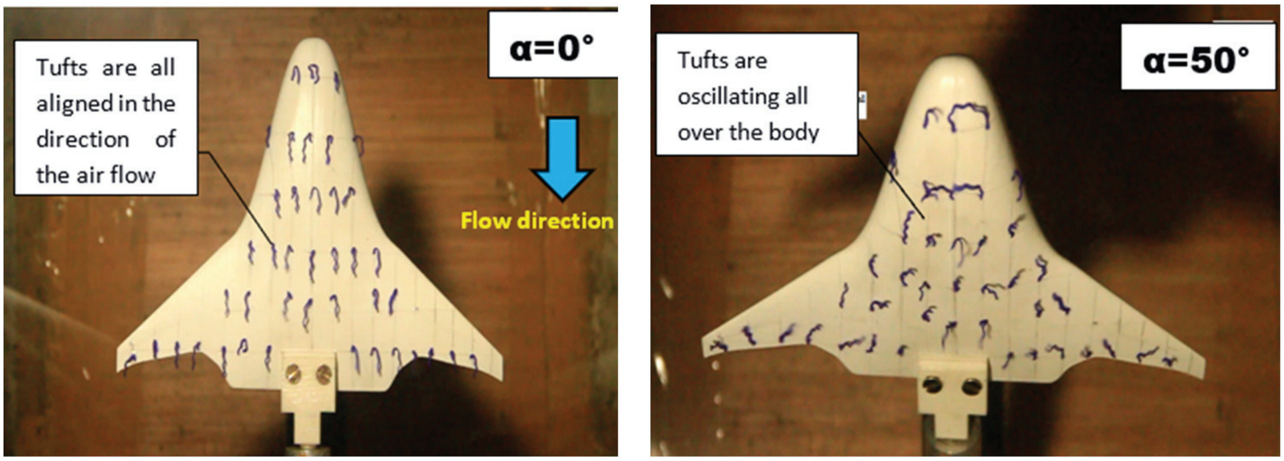

(a) AoA = 0^0 (b) AoA = 50^0

Figure 10. Tuft Flow Visualisation at different angles of attack.

CAD model is used to fabricate a 3-D model using a 3-D printer. In the present work, numerical simulations are carried out using an open-source CFD software OpenFOAM. The variations of lift, drag, and lift/drag (L/D) ratio with AoA are investigated. It is observed that the AoA at the stall for this BWB configuration is around 45^{o}. This happens due to the fact that the wing stalls at low AoA, but the body still produces lift with increasing AoA. Hence, the aircraft body is the main contributor to lift at high AoA. The coefficient of drag (C_D) continues to increase with AoA due to the spreading of the separated region over the BWB geometry. The variation of the lift/drag (L/D) ratio with AoA is also studied. The maximum L/D ratio for this BWB configuration is observed at around eight at an AoA = 6^0. This suggests the optimum flight configuration of the present BWB is at AoA = 6^0 for better aerodynamic performance. To investigate the flow over this BWB geometry, the sectional pressure distribution at different spanwise locations, velocity contours, pathlines, surface limiting streamlines and tuft flow visualization are also presented for different AoA. Further studies can be performed to investigate the aerodynamic stability of this type of BWB geometry. More research is also required for a detailed analysis of flow physics under different operating conditions.

REFERENCES

1. Liebeck, R.H. Design of the blended wing body subsonic transport. *J. Aircraft*, 2004**, 41**(1), 10–25. doi: 10.2514/1.9084
2. Potsdam, M.A.; Page, M.A. & Liebeck, R.H. Blended wing body analysis and design. AIAA Paper 1997-2317, 1997. doi: 10.2514/6.1997-2317
3. Martinez, R.M. Design and analysis of the control and stability of a blended wing body aircraft. M. Sc. Thesis, Royal Institute of Technology (KTH), 2014.
4. Carlsson, M. & Kuttenkeuler, J. Design and testing of a blended wing body aeroelastic wind-tunnel model. *J. Aircraft*, 2003, **40**(1), 211-214. doi: 10.2514/2.3079
5. Qin, N.; Vavalle, A.; Moigne; A. L.; Laban, M.; Hackett, K. & Weinerfelt, P. Aerodynamic considerations of blended wing body aircraft. *Progress in Aerospace Sci.*, 2004, **40**(6), 321–343. doi: 10.1016/j.paerosci.2004.08.001
6. Re, R.J. Longitudinal aerodynamic characteristics and wing pressure distributions of a blended wing body configuration at low and high reynolds numbers. NASA/TM-2005-213754, 2005.
7. Ammar, S.; Legros, C. & Trépanier, J.Y. Conceptual design, performance, and stability analysis of a 200 passengers Blended Wing Body aircraft*. Aerospace Sci. Technol.*, 2017, **71**, 325–336. doi: 10.1016/j.ast.2017.09.037
8. OpenFOAM® - Official home of The Open Source Computational Fluid Dynamics (CFD) Toolbox: http://www.openfoam.com/ (Accessed on April 2019).
9. NACA 4-digit airfoil generator: http://airfoiltools.com/airfoil/naca4digit/ (Accessed April 2019).
10. Dehpanah, P. & Nejat, A. The aerodynamic design evaluation of a blended-wing-body configuration. *Aerospace Sci. Technol.*, 2015, **43**, 96–110. doi: 10.1016/j.ast.2015.02.015
11. Thompson, D.J.; Feys, J.; Filewich, M.D.; Magid, S.A.; Dalli, D. & Goto, F. The design and construction of a blended wing body UAV. AIAA Paper 2011-841, 2011. doi: 10.2514/6.2011-841
12. Roman, D.; Gilmore, R. & Wakayama, S. Aerodynamics of high subsonic blended-wing-body configurations. AIAA Paper 2003-554, 2003. doi: 10.2514/6.2003-554
13. Lyu, Z. & Martins, J.R.R.A. RANS-based aerodynamic shape optimization of a blended wing-body aircraft. AIAA Paper 2013-2586, 2013. doi: 10.2514/6.2013-2586
14. Okonkwo, P. & Smith, H. Review of evolving trends in blended wing body aircraft design. *Progress in Aerospace Sci.*, 2016**, 82**, 1–23. doi: 10.1016/j.paerosci.2015.12.002
15. Kuntawala, N.B.; Hicken, J.E. & Zingg, D.W. Preliminary aerodynamic shape optimization of a blended-wing-body aircraft configuration. AIAA Paper 2011-642, 2011. doi: 10.2514/6.2011-642

16. Larkin, G. & Coates, G. A design analysis of vertical stabilizers for blended wing body aircraft. *Aerospace Sci. Technol.*, 2017, **64**, 237-252. doi: 10.1016/j.ast.2017.02.001
17. Zhang, M.; Rizzi, A.; Meng, P.; Nangia, R.; Amiree, R. & Amoignon, O. Aerodynamic design considerations and shape optimization of flying wings in transonic flight. AIAA Paper 2012-5402, 2012. doi: 10.2514/6.2012-5402
18. Siouris, S. & Qin, N. Study of the effects of wing sweep on the aerodynamic performance of a blended wing body aircraft. Proceedings of the Institution of Mechanical Engineers, Part G. *J. Aerospace Eng.,* 2007, **221**(1), 47–55. doi: 10.1243/09544100JAERO93
19. Howe, D. Blended wing body airframe mass prediction. Proceedings of the Institution of Mechanical Engineers, Part G. *J. Aerospace Eng.*, 2001**, 215**(6), 319–331. doi: 10.1243/0954410011533329
20. Nguyen, N.; Choi, S.; Kim, W.; Lee, J.; Kim, S.; Neufeld, D. & Byun, Y. Multidisciplinary unmanned combat air vehicle system design using multi-fidelity model. *Aerospace Sci. Technol.*, 2013, **26**(1), 200-210. doi: 10.1016/j.ast.2012.04.004
21. Nguyen, N.; Lee, D.; Tyan, M.; Lee, J. & Kim, S. Efficient stall compliance prediction method for trimmed very light aircraft with high-lift devices. Proceedings of the Institution of Mechanical Engineers, Part G. *J. Aerospace Eng.*, 2017, **231**(6), 1124-1137. doi: 10.1177/0954410016648981
22. Torenbeek, E. Blended-wing-body aircraft: A historical perspective. Encyclopedia of Aerospace Engineering, 2016. doi:10.1002/9780470686652.eae1003
23. Vicroy, D.D; Murri, D.G; & Abeyounis, W.K. Low-speed aerodynamic characteristics of a subsonic blended-wing-body tri-jet configuration. NASA TM-2006-214309, May 2006.
24. Wisnoe, W.; Nasir, R.E.M.; Kuntjoro, W. & Mamat, A.M.I. Wind tunnel experiments and CFD Analysis of Blended Wing Body (BWB) Unmanned Aerial Vehicle (UAV) at Mach 0.1 and Mach 0.3. *In* 13th International Conference on Aerospace Sciences & Aviation Technology, ASAT-13, 2009.
25. Nasir, R.E.M.; Kuntjoro, W. & Wisnoe, W. Aerodynamic, stability and flying quality evaluation on a small blended wing-body aircraft with canard foreplanes, *Procedia Technology,* 2014, **15**, 783 – 791, doi: 10.1016/j.protcy.2014.09.051
26. Brown, M. & Vos, R. Conceptual design and evaluation of blended-wing-body aircraft. AIAA Paper 2018-0522, 2018. doi: 10.2514/6.2018-0522
27. Zadeh, P.M. & Sayadi, M. An efficient aerodynamic shape optimization of blended wing body UAV using multi-fidelity models. *Chinese J. Aeronautics,* 2018, **31**(6), 1165–1180. doi: 10.1016/j.cja.2018.04.004
28. Lyu, D.; Song, B.; Pan, G.; Yuan, Z. & Li, J. Winglet effect on hydrodynamic performance and trajectory of a blended-wing-body underwater glider. *Ocean Engineering,* 2019, **188**, 106303. doi: 10.1016/j.oceaneng.2019.106303
29. Zhang, M.; Chen, Z.; Tan, Z.; Gu, W.; Li, D.; Yuan, C. & Zhang, B. Effects of stability margin and thrust specific fuel consumption constraints on multidisciplinary optimization for blended-wing-body design. *Chinese J. Aeronautics,* 2019, **32**(8), 1847–1859. doi: 10.1016/j.cja.2019.05.018
30. Viviani, A.; Aprovitola, A.; Iuspa, L. & Pezzella, G. Low-speed longitudinal aerodynamics of a blended wing-body re-entry vehicle. *Aerospace Sci. Technol.,* 2020, **107**, 106303. doi: 10.1016/j.ast.2020.106303
31. Wang, G.; Zhang, M.; Tao, Y.; Li, J.; Li, D.; Zhang, Y.; Yuan, C.; Sang, W. & Zhang, B. Research on analytical scaling method and scale effects for subscale flight test of blended wing body civil aircraft. *Aerospace Sci. Technol.,* 2020, **106**, 106114. doi: 10.1016/j.ast.2020.106114
32. Kapsalis, S.; Panagiotou, P. & Yakinthos, K. CFD-aided optimization of a tactical Blended-Wing-Body UAV platform using the Taguchi method. *Aerospace Sci. Technol.,* 2021, **108**, 106395. doi: 10.1016/j.ast.2020.106395
33. Spalart, P.R. & Allmaras, S.R. A one-equation turbulence model for aerodynamic flows. AIAA Paper 1992-0439, 1992. doi: 10.2514/6.1992-439
34. Kumar, P. & Prasad, J.K. Mechanism of side force generation and its alleviation over a slender body. *J. Spacecraft and Rockets*, 2016, **53**(1), 195 – 208. doi: 10.2514/1.A33290
35. Versteeg, H.K. & Malalasekera, W. An introduction to computational fluid dynamics: The finite volume method. Pearson Education, Harlow, 2007.
36. Blazek, J. Computational Fluid Dynamics: Principles and applications. Elsevier, 2001.

ACKNOWLEDGMENT

We wish to thank Mr Avik Arora, Master's student, Department of Space Engineering and Rocketry, BIT Mesra, Ranchi, for his constant support and help during the fabrication process with the 3D printing technology.

CONTRIBUTORS

Mr Midhun MV obtained his ME in Aerodynamics from Birla Institute of Technology, Mesra, Ranchi. He has working experience in Computational Fluid Dynamics as well as Experimental Aerodynamics.
His current role was to perform computations and experiments in the present work.

Dr Partha Mondal obtained his PhD in Aerospace Engineering from Indian Institute of Science, Bangalore. He is working as an Assistant Professor at the Department of Space Engineering

and Rocketry, Birla Institute of Technology, Mesra, Ranchi. His areas of research include: Aerodynamics, Computational Fluid Dynamics.
His current role was for this work to guide and help in performing computations and experiments.

Mr Pawan Kumar Karn obtained his PhD in the field of Aerodynamics from the Department of Space Engineering and Rocketry, Birla Institute of Technology, Mesra, Ranchi. He has working experience in Computational Fluid Dynamics as well as Experimental Aerodynamics.
His current role was to perform experiments in the present work.

Dr Priyank Kumar is currently working as an Assistant Professor in the Department of Space Engineering & Rocketry, Birla Institute of Technology, Mesra, Ranchi. His research areas are Fluid dynamics, Aerodynamics and Low-speed flow.
His current role was to guide and help in performing experiments for this work.